Ｖ１の構造と機能

by　北岡明佳

Ｖ１（visual area 1）＝視覚一次野、線条皮質（striate cortex）

①投射　　外側膝状体（ＬＧＮ）→**V1**→Ｖ２、ＭＴなど

②網膜対応性（retinotopic organization）
　　視野中心（fovea）近くが拡大され、周辺（periphery）は縮小される。

　　視野地図（retinotopic map）
　　受容野（receptive field）
　　拡大因子（magnification factor）
　　ポイントイメージ（point image）

③大細胞系と小細胞系（magnocellular and parvocellular systems）
　　ＬＧＮmagnocellular layer→４Ｃα→４Ｂ→Ｖ２thick stripe、ＭＴ
　　ＬＧＮparvocellular layer→４Ｃβ→４Ａ→２／３層→Ｖ２pale stripe
　　視力（acuity）、空間周波数（spatial frequency）
　　コントラスト感受性（contrast sensitivity）
　　時間周波数（temporal frequency）

④コラム構造（columnar structure）
　　眼優位コラム（ocular dominance column）
　　方位選択性コラム（orientation column）
　　チトクロームオキシダーゼブロッブ（CO blob）
　　空間周波数コラム（spatial frequency column）
　　超コラム（hypercolumn）の変遷

方位選択性ニューロンの分類
１．単純型（simple）
２．複雑型（complex）
３．超複雑型（hypercomplex）

⑤V1 以降

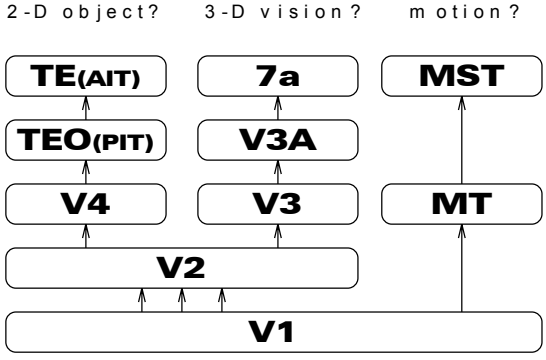

視野地図
(retinotopic map)

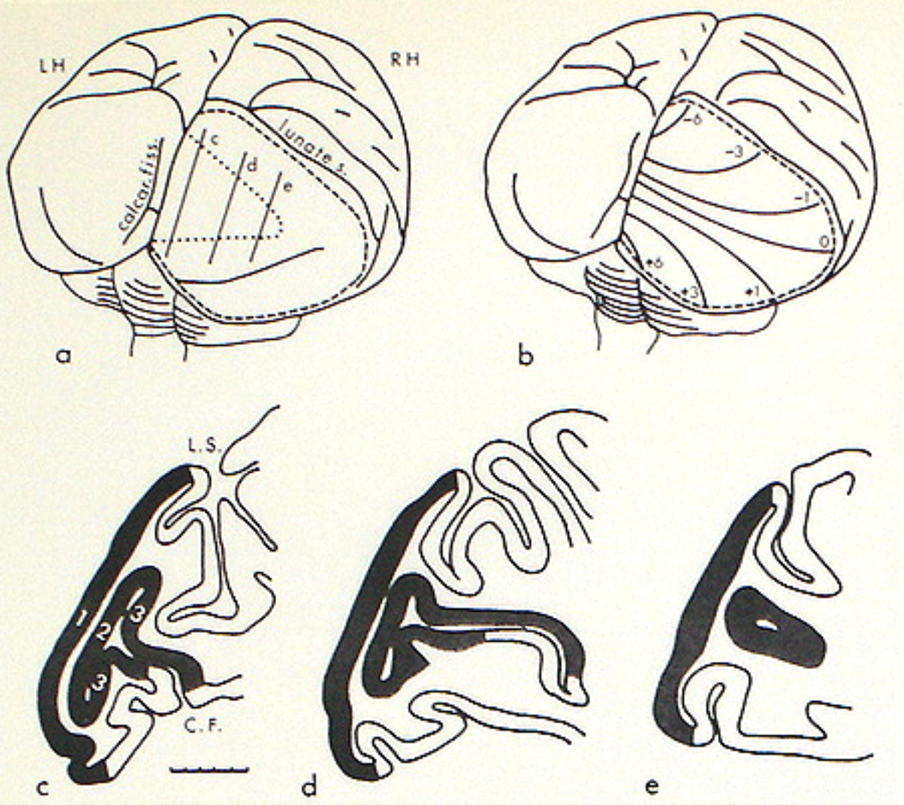

from Hubel et al. (1978)

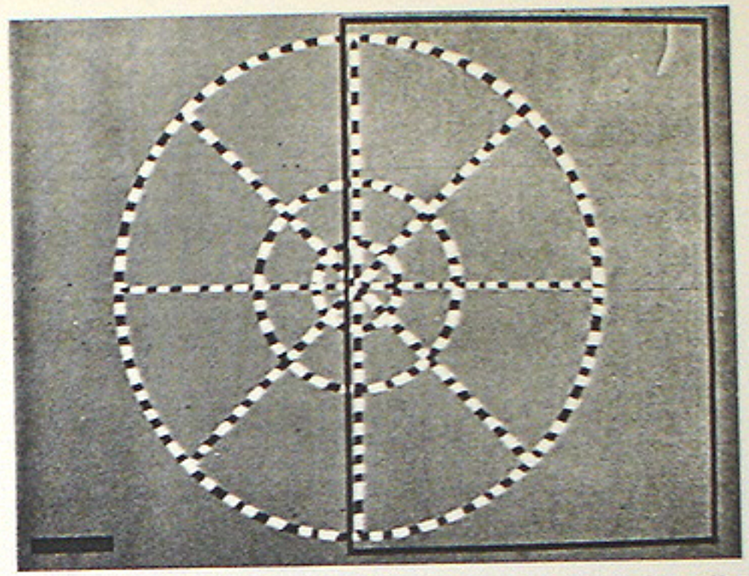

Figure 1. One of the stimuli used in the DG mapping study. During the actual experiment, the black and white checks reversed in contrast (that is, changed from black to white and back) in a temporal square wave at 3 Hz. The luminance of the unvarying gray background was equal to the time-averaged mean luminance of the flickering black and white checks (85.7 cd/m²). The stimulus was centered on the animal's fovea. The first ring is at 1°, the second ring at 2.3°, and the third at 5.4°. The *solid black rectangle* enclosing slightly more than half of the stimulus was not in fact part of the original stimulus; instead, it indicates that portion of the visual field projecting to one hemisphere (see Fig. 2). Calibration bar, 2° in the visual field.

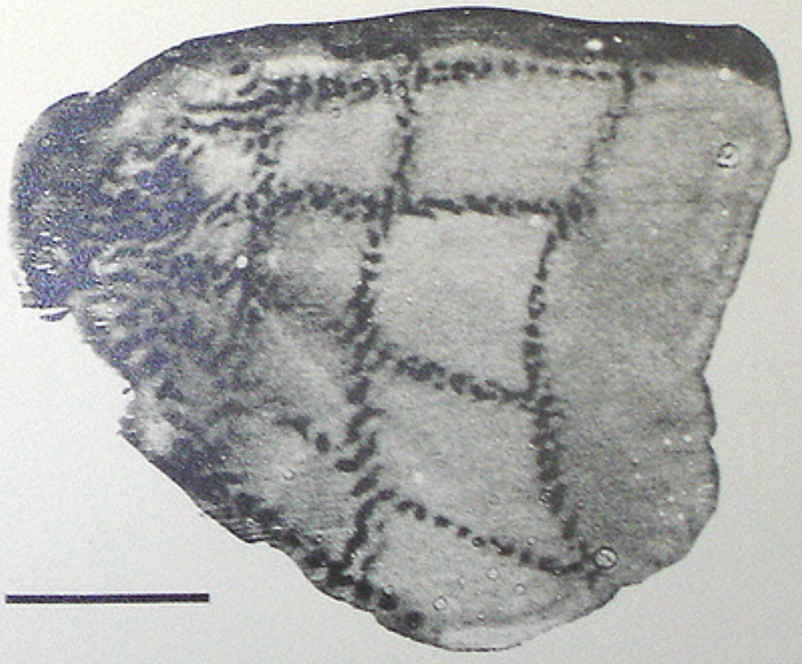

Figure 2. DG autoradiographs showing the effect of the retinotopic stimulus (Fig. 1) in various layers. The section in *A* cuts through layers 2 + 3, and the section in *B* is mostly from layer 4C. Both are tangential sections cut from the same flattened operculum, representing eccentricities from about 0°–7°. The fovea is represented towards the *left* and the periphery is represented towards the *right*. The DG retinotopic borders are more sharply defined and higher in contrast in layer 4C (*B*) than in the upper striate layers (*A*), especially towards the periphery, where the cortical representation of stimulus checks becomes smaller. Scale bar, 1 cm.

from Tootell et al. (1988)

Retinal representation in V1

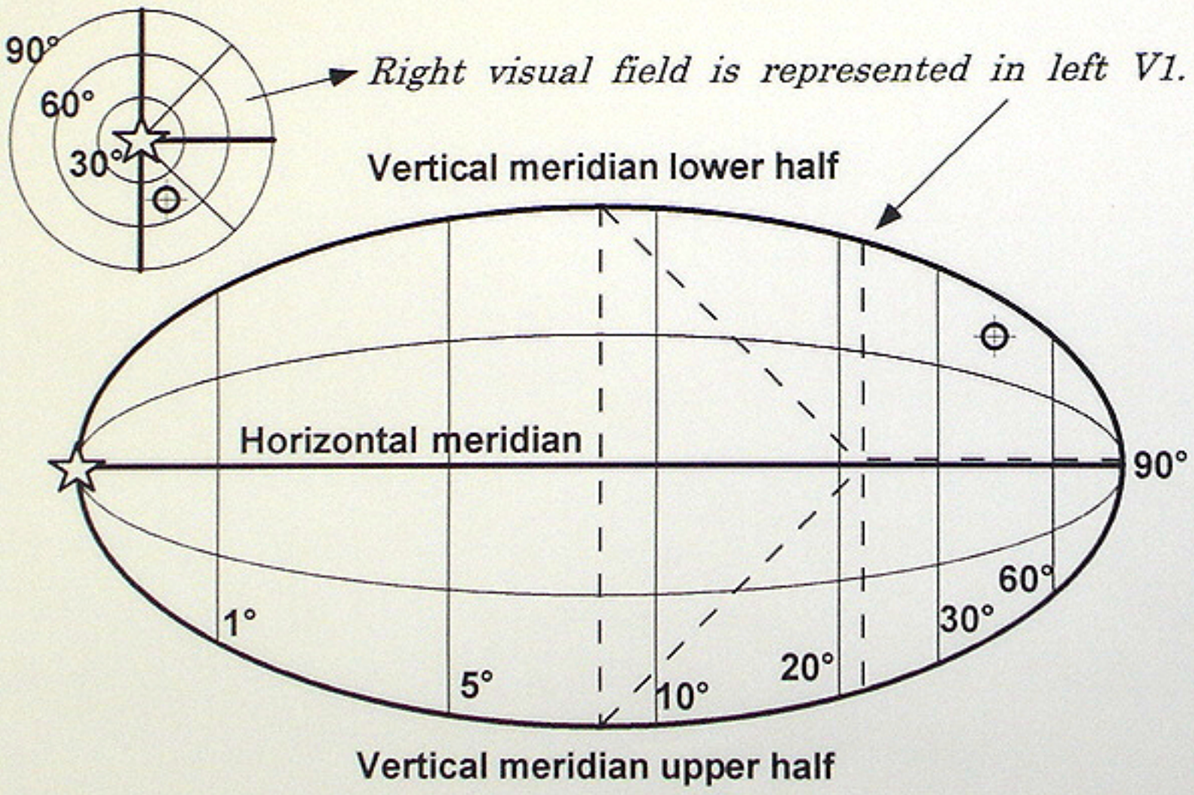

From Daniel and Whitteridge (1961)

眼優位コラム
(ocular dominance column)

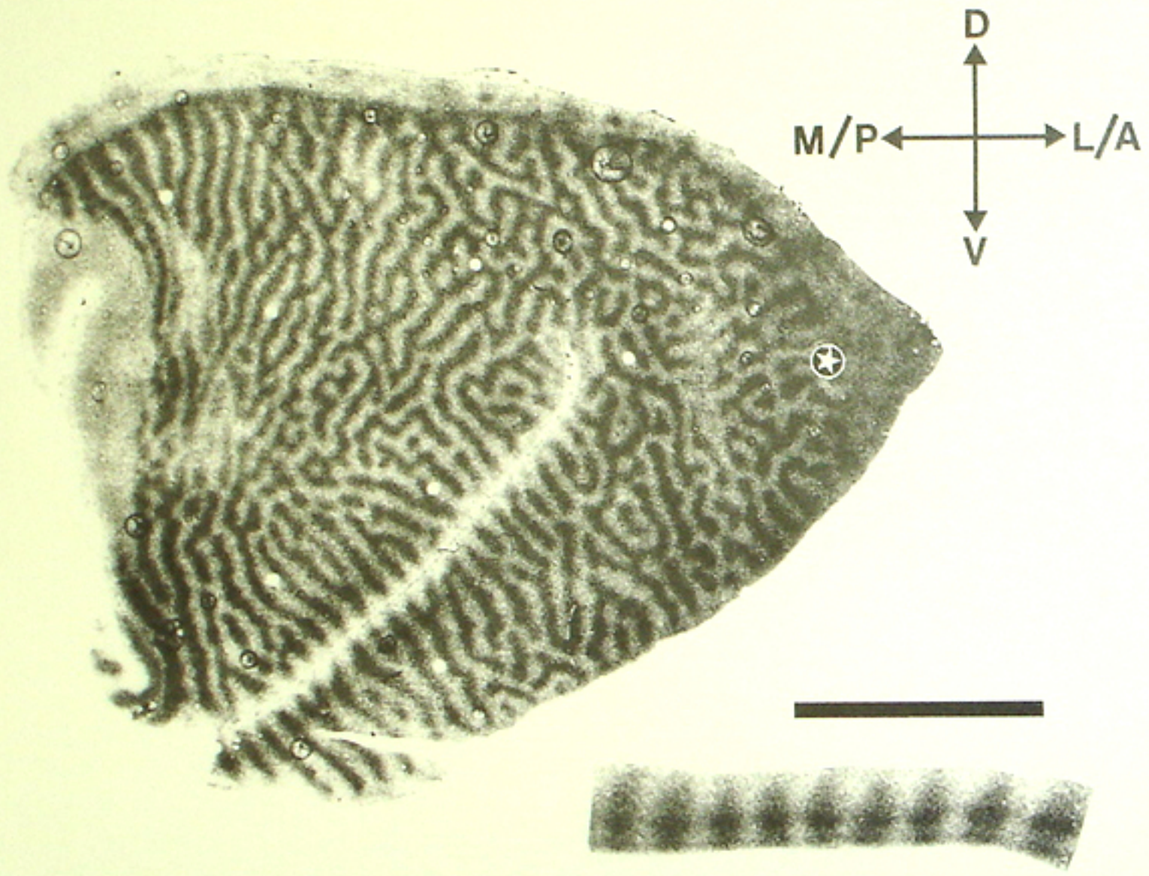

Figure 2. Deoxyglucose autoradiograph showing ocular dominance strips in macaque striate cortex, mostly from layer 3. The stimulus producing this DG pattern was a moving, black and white square-wave grating of varied spatial frequency, shown at different orientations to one eye. Such a stimulus produces long strips of high DG uptake in all layers that run generally perpendicular to the 17–18 border. The large section shown in this figure was cut parallel with the lateral surface of the unfolded, flat-mounted operculum, and it includes about half the surface area of striate cortex. In this and other illustrations, sections from striate cortex that are unfolded are roughly triangular in shape, with the representation of the fovea at the apex of the triangle (indicated by a *star*), and the posterior edge of the operculum (representing about 7° eccentricity) at the base of the triangle along the left-hand side of the picture. The orientation of this section *in vivo* is roughly indicated by the set of *arrows* in the upper right. *D*, dorsal, *V*, ventral, *M/P*, medial/posterior, *L/A*, lateral/anterior. *Inset, lower right*, Laminar distribution of DG uptake in ocular dominance columns in a section cut perpendicular to the cortical surface. The inset is magnified 2× relative to the large section. Scale bar, 1 cm relative to large section, 5 mm relative to inset.

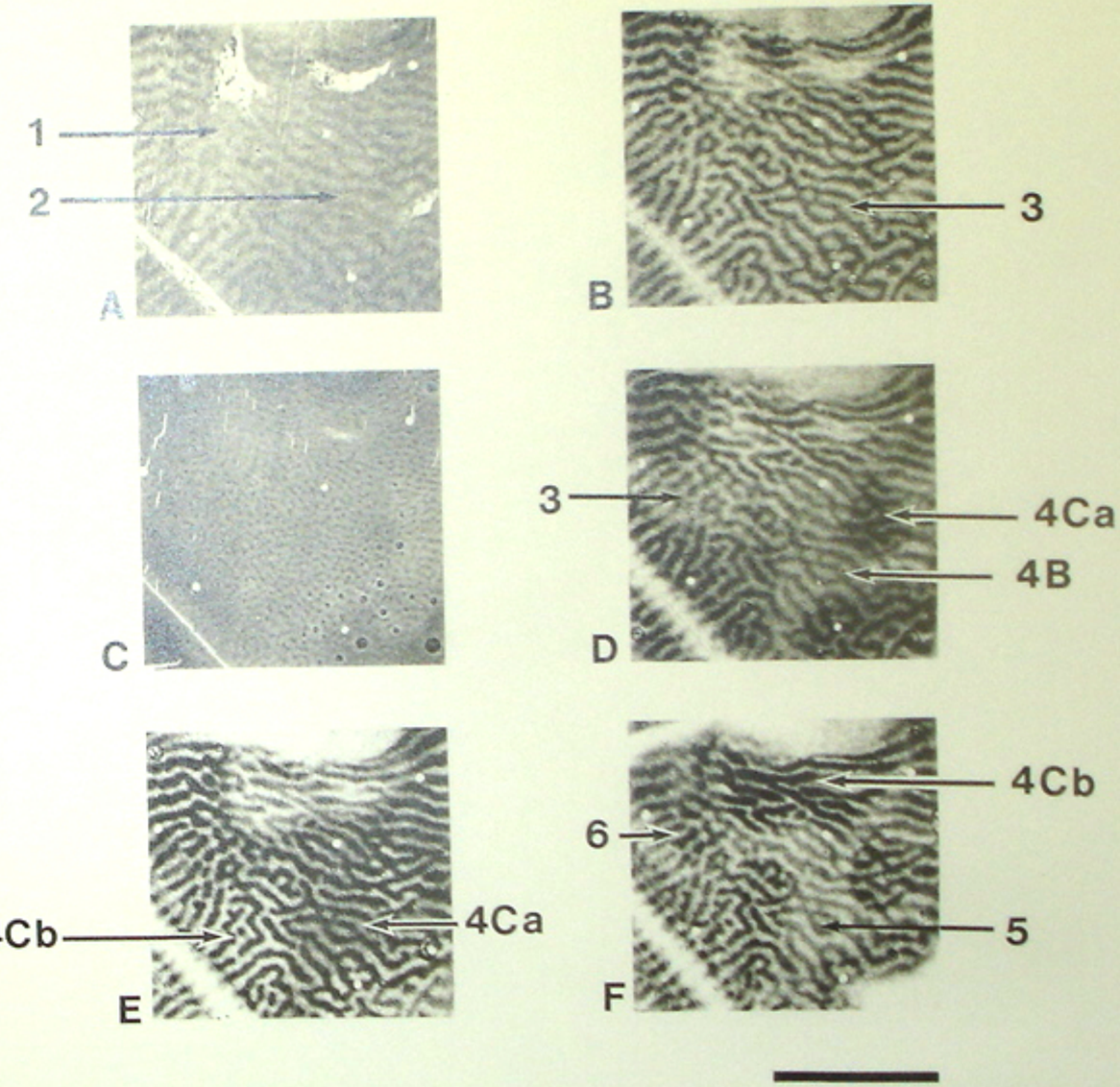

Figure 3. Laminar variations in DG ocular dominance columns. *A, B, D–F*, DG patterns in the same area of cortex from successively deeper sections. The topography of the DG ocular dominance columns remains relatively constant across different layers, although levels of uptake in the stimulated and unstimulated eye dominance columns vary widely. Of special note are the presence of ocular dominance columns in layer 1 (*A*) and a significant level of stimulus-induced uptake in the light ("unstimulated") eye dominance columns in 4Ca (*E*). A similar pattern of stimulus-induced uptake does not occur in the light ocular dominance strips in layer 4Cb, nor in other layers. *C*, The same section used in *B*, stained for cytochrome oxidase and shown at the same scale. Clearly, the layer 3 ocular dominance strips in *B* are wider and more uniform in width (that is, more "striplike") than the blobs shown in *C*. Calibration bar, 1 cm.

from Tootell et al. (1988)

方位選択性コラム 1
(orientation column)
- electrophysiology -

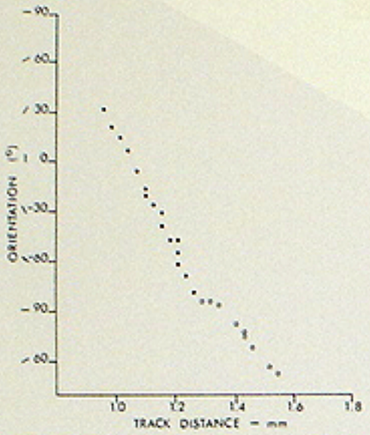

Fig. 1B Graph of orientation vs. track distance for the sequence of figure 1A. In plotting orientations, 0° is vertical, angles clockwise up to 90° are positive, counterclockwise to 89°, negative. Closed circles, ipsilateral (right) eye; open circles, contralateral (left) eye. Track distance is taken from micrometer advancer readings.

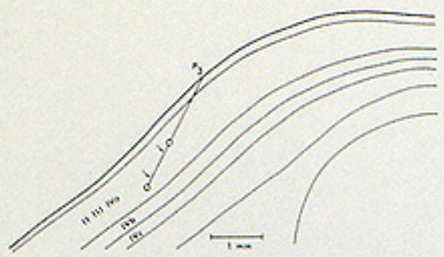

Fig. 1C Reconstruction of the electrode track. Electrode entered the striate cortex 8 mm behind the lunate sulcus in the parasagittal plane, 10 mm to the right of the midline, intersecting the surface at 20°. The sequence described here was recorded between the two arrows. Circles represent electrolytic lesions. Anterior is to the right.

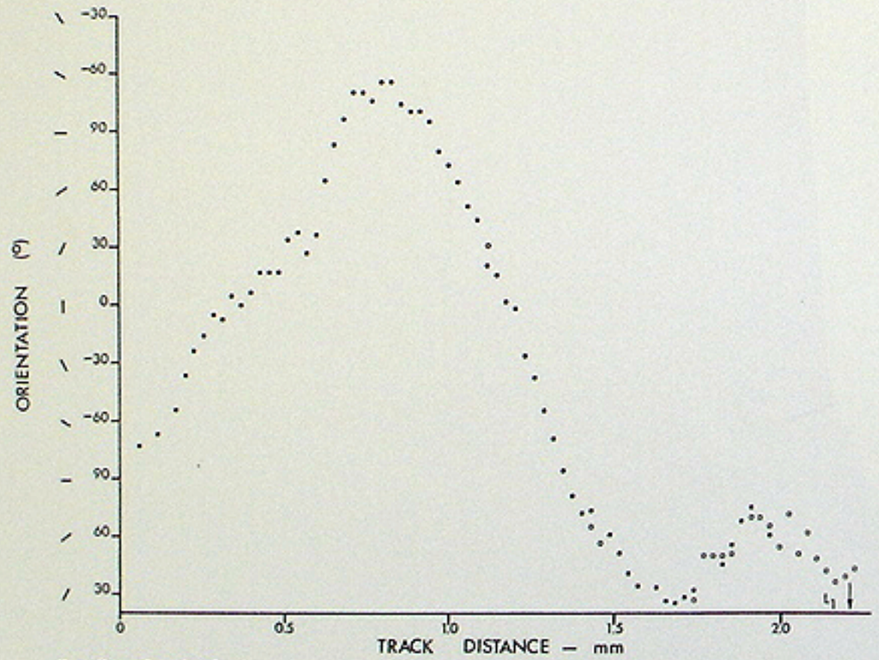

Fig. 2A Graph of orientation vs. track distance for an oblique penetration through striate cortex in a normal monkey. Note the reversals in direction of orientation shifts, the first two of which bracket a long sequence spanning 267°. (Experiment No. 7.)

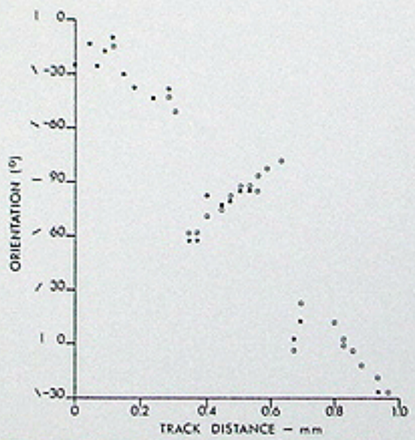

Fig. 3 Graph of orientation vs. track distance for a sequence that showed two clear breaks in regularity (Experiment No. 5, penetration 2; see fig. 8C).

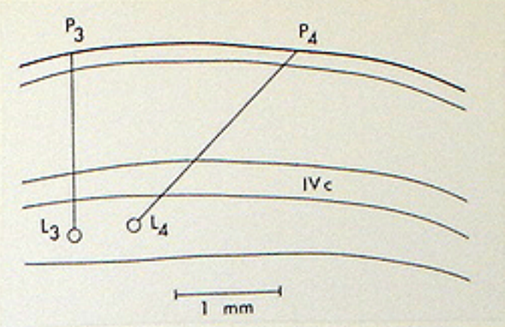

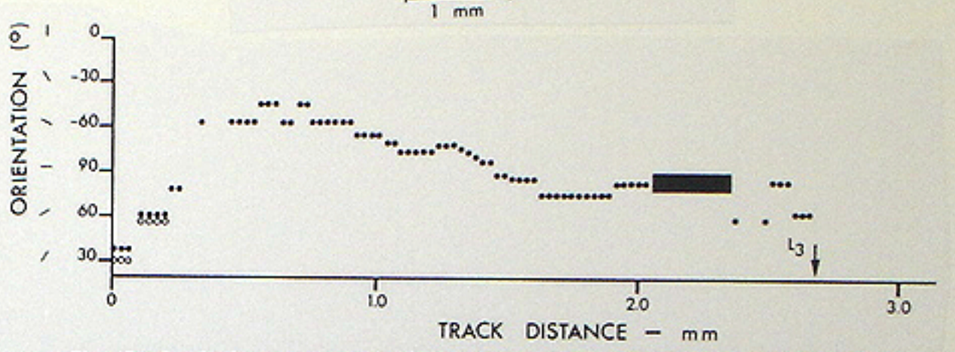

Fig. 4B Graph of orientation vs. track distance for the perpendicular penetration P3. Slope −54°/mm, uncorrected for angle to surface. The filled dark bar represents activity in layer IV C, which was influenced exclusively from the ipsilateral eye and showed no orientation selectivity; the bar's placement along the orientation axis is arbitrary.

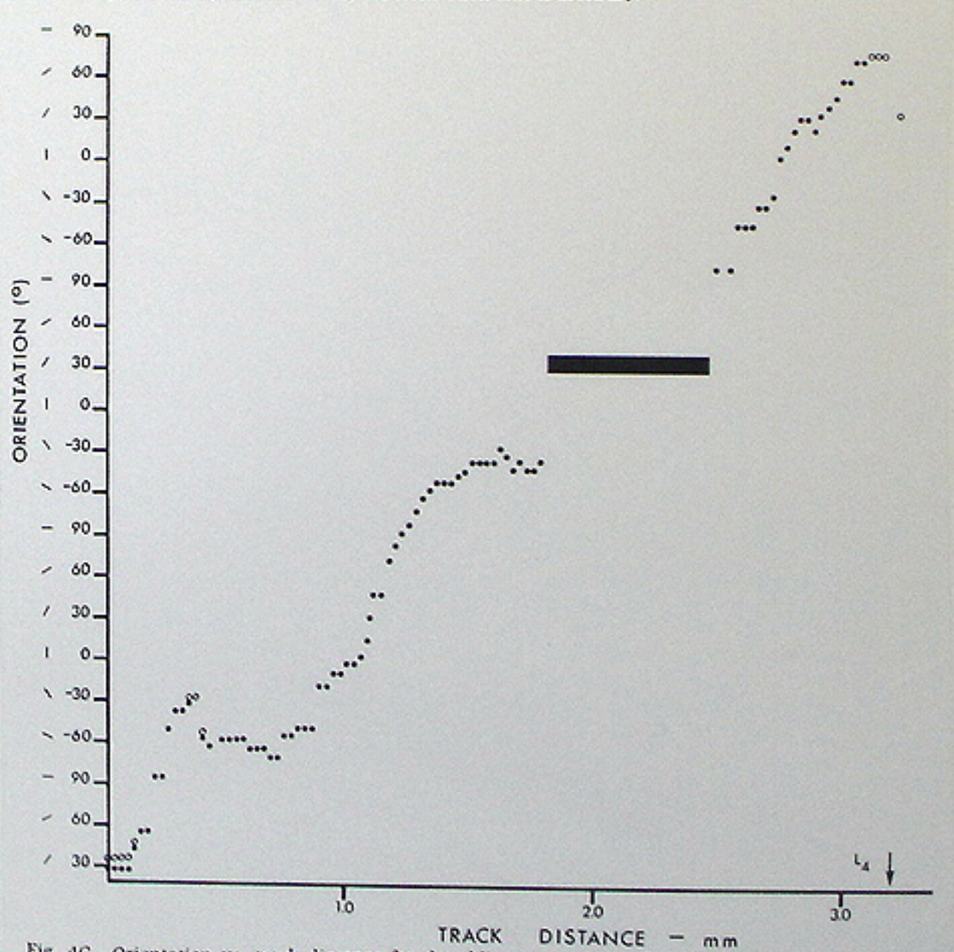

Fig. 4C Orientation vs. track distance for the oblique penetration P4. Slope, 273°/mm, uncorrected.

from Hubel and Wiesel (1974)

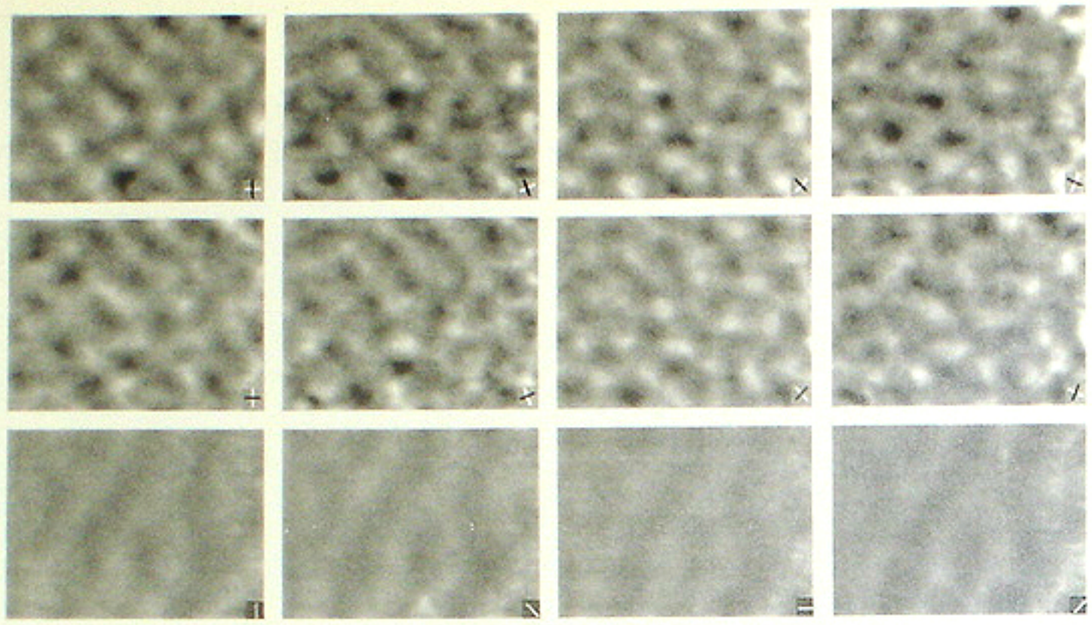

Figure 7. *Top two rows,* Each frame in the upper rows reveals a differential image of orientation, obtained by comparing cortical images acquired during stimulation with one orientation and its orthogonal. Preferences for the orientations indicated by dark and light bars (*lower right corner*), appear as dark and light values in each image. Successive images were acquired with both contours rotated through 22.5° between frames. As one can easily verify, the images lying above one another, which are offset by 90°, are complimentary (see Results). In any particular frame, one can usually see short bands, running in particular directions. Nevertheless, when the stimulus orientations are rotated slightly, the apparent bands do not move laterally (as one might expect from the model in Fig. 2*b*), but break apart and form new patterns that run in different directions. *Bottom row,* Differential images of ocular dominance, obtained by subtracting frames of cortex responding to the left eye from frames of it responding to the right. Each of these images was obtained with visual stimuli at a different orientation (indicated in the *lower right corner*).

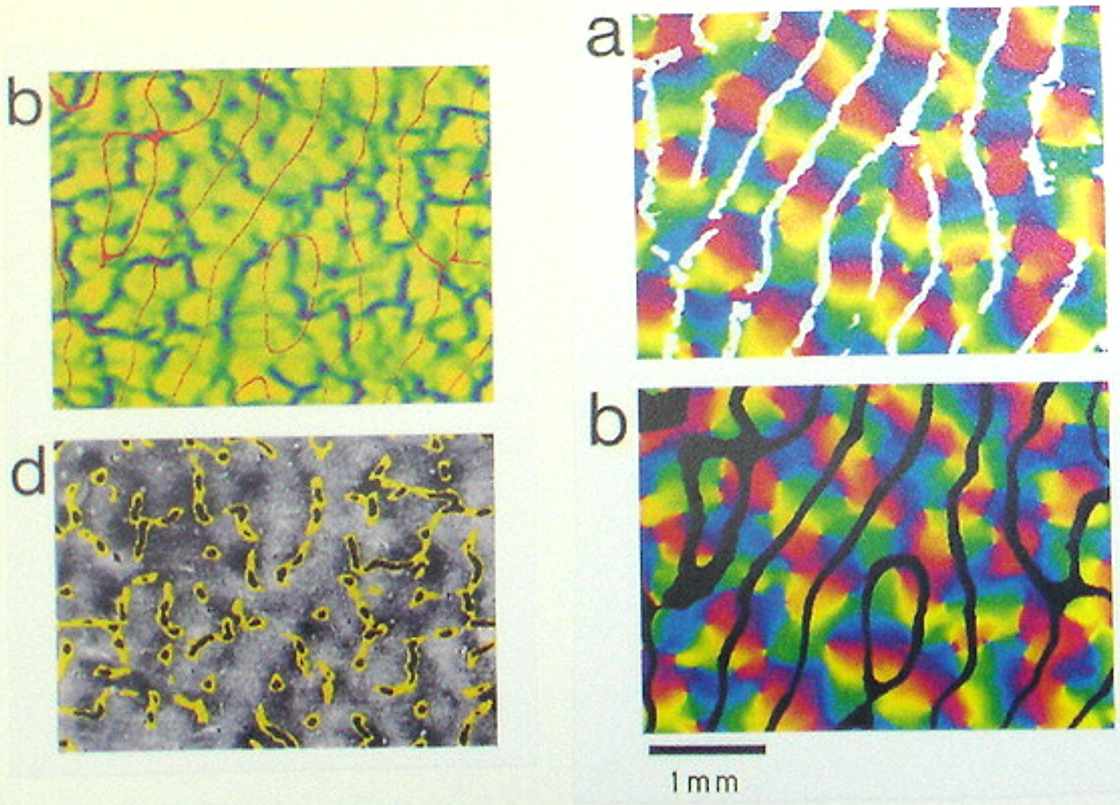

方位選択性コラム 2
(orientation column)
- optical recording -

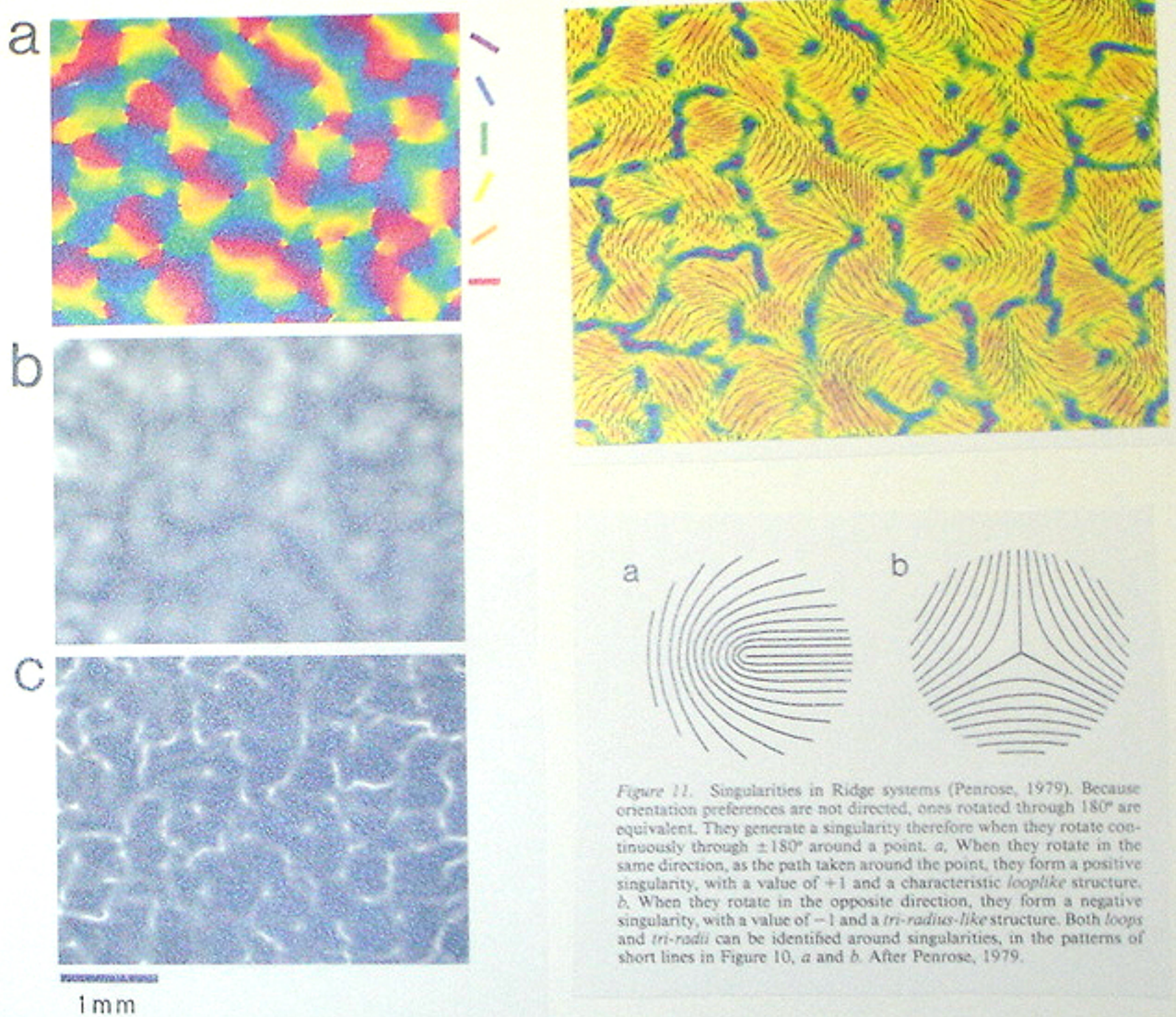

Figure 7. When the differential images in Figure 5 are combined, they produce similar maps of orientation preference and selectivity, which appear in *a* and *b*. As in Figure 6, orientation preferences (*a*) must be illustrated in color because they cycle continuously through 180°. Complimentary colors indicate orthogonal orientations: *green* and *red* indicate preferences for vertical and horizontal, while *blue* and *yellow* indicate preferences for left and right oblique. Orientation selectivity (*b*) is indicated in gray, with *lighter* and *darker* regions indicating more and less selectivity. As noted in the Results, *light values* are unambiguous—they indicate strongly responsive regions that were highly selective—while darker values might indicate regions that were nonresponsive as well as ones that were nonselective. Since many of the dark regions are aligned with ocular dominance centers, though, where responses to one or the other eye are pronounced, they would appear to result from a lack of orientation selectivity since these regions obviously are responsive to the visual stimuli used. In *c*, one sees the absolute magnitude of the orientation gradient at each location, which corresponds to the rate at which orientation preferences are changing between pixels. While the gradient is a *linear* operator, defined only in regions of continuous change, it is calculated from discrete values that change

Figure 11. Singularities in Ridge systems (Penrose, 1979). Because orientation preferences are not directed, ones rotated through 180° are equivalent. They generate a singularity therefore when they rotate continuously through ±180° around a point. *a*, When they rotate in the same direction, as the path taken around the point, they form a positive singularity, with a value of +1 and a characteristic *looplike* structure. *b*, When they rotate in the opposite direction, they form a negative singularity, with a value of −1 and a *tri-radius-like* structure. Both *loops* and *tri-radii* can be identified around singularities, in the patterns of short lines in Figure 10, *a* and *b*. After Penrose, 1979.

←

in any case and that can be used to visualize discontinuities. As one can see in this image, discontinuous changes either occur alone, at points, or they group together along lines. The zero-dimensional discontinuities, at points, indicate *singularities,* where orientation preferences change by more than 90° between pixels, and which arise at the centers of vortices where orientation preferences rotate continuously through ±180°. Short one-dimensional lines indicate *fractures,* where preferences change discontinuously by *less* than 90°, and which run between adjacent regions of cortex where orientation preferences change linearly.

from Blasdel (1992)

COブロッブ
(CO blob)

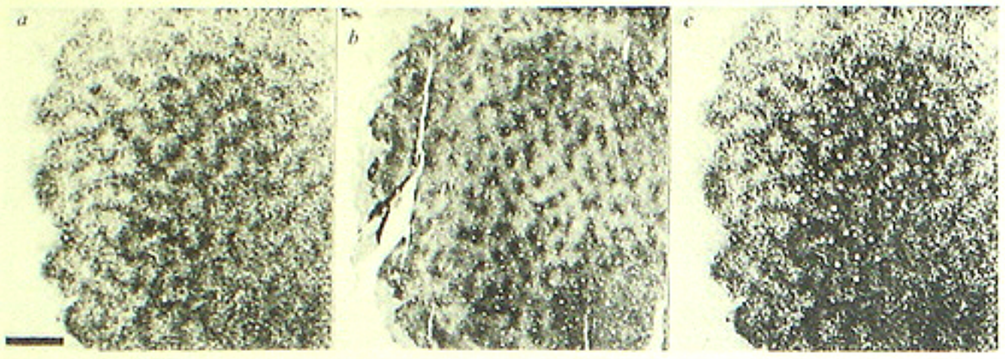

Fig. 4 *a*, Complex pattern of ^{14}C-2-deoxyglucose label in layers II, III of macaque striate cortex after stimulation of both eyes with vertical stripes. *b*, An adjacent section stained for cytochrome oxidase shows an array of patches. *c*, The cytochrome oxidase patches fall within the lattice of deoxyglucose label, as shown by representing each patch in *b*, with a small white dot, and placing them directly on *a*. Scale bar, 1 mm.

└ from Horton and Hubel (1981) ——

└ from Tootell et al. (1988) ——

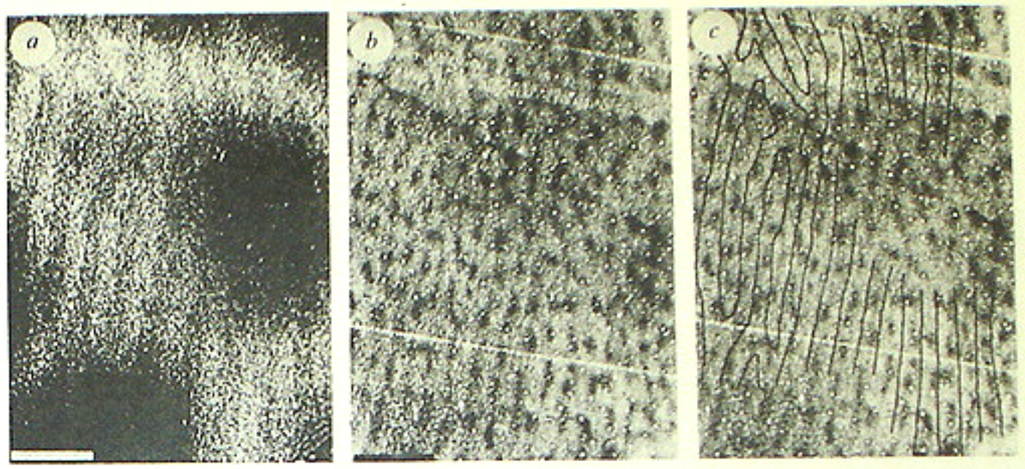

Fig. 2 *a*, Dark-field autoradiograph of striate cortex in a normal monkey whose right eye was injected with ^{3}H-proline 2 weeks earlier. The section is tangential, grazing layer V (dark ovals) but passing mainly through layer IVc. Here typical ocular dominance columns are seen as light bands of label corresponding to the injected eye separated by darker gaps. *b*, More superficial section from the same block as *a*, cytochrome oxidase stain. The rows of cytochrome oxidase patches in the superficial layers follow the pattern of the ocular dominance patches. This is shown in *c* by drawing the borders of the columns from *a* directly onto *b*. Scale bar, 1 mm.

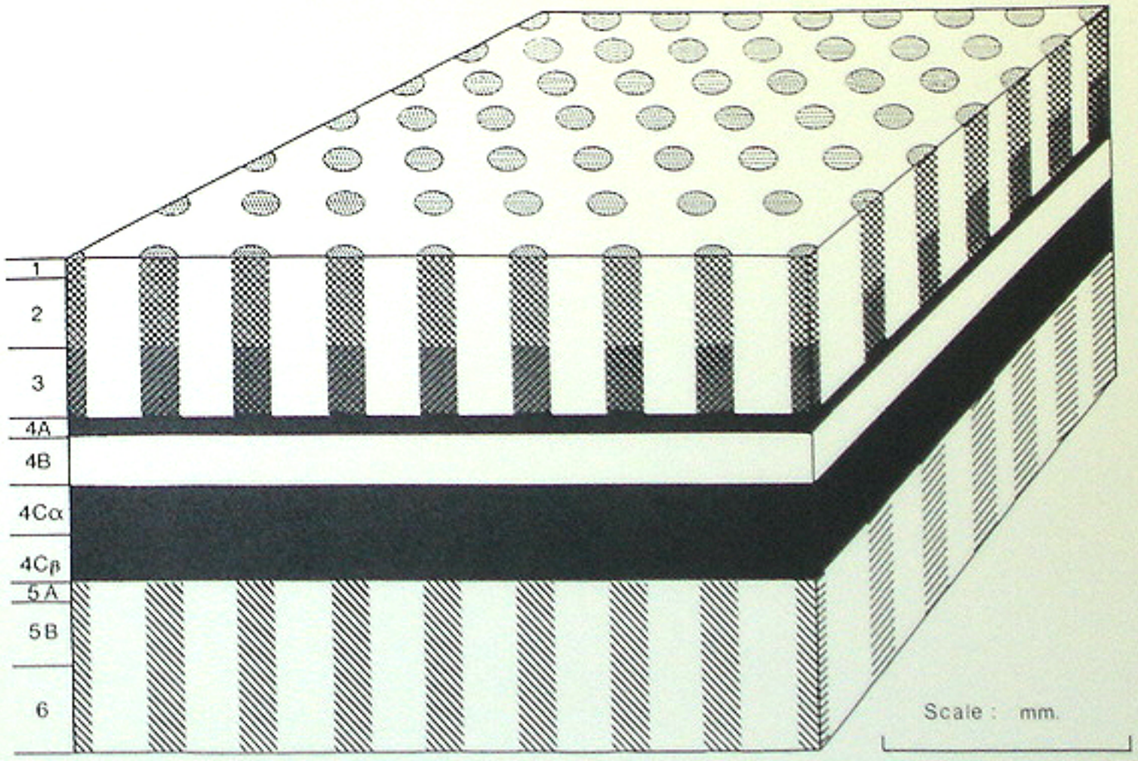

Figure 1. Diagram of the cytochrome oxidase architecture in macaque striate cortex. The cytochrome oxidase "blobs" (also described as "puffs" or "patches") are found in all layers outside of layer 4 and marginally in layer 4B. The various *stippling patterns* in the diagrammatic blobs in each of the indicated layers give some idea of the corresponding contrast of the blobs *in vivo*. The blobs are most obvious in layer 3, less so in layer 2, and fainter in layers 1, 5, and 6. In some cases, the blobs are marginally visible, and in others, they are invisible, as in layer 4B (indicated by a lack of stippling). Scale bar, 1 mm.

超コラム
(hypercolumns)

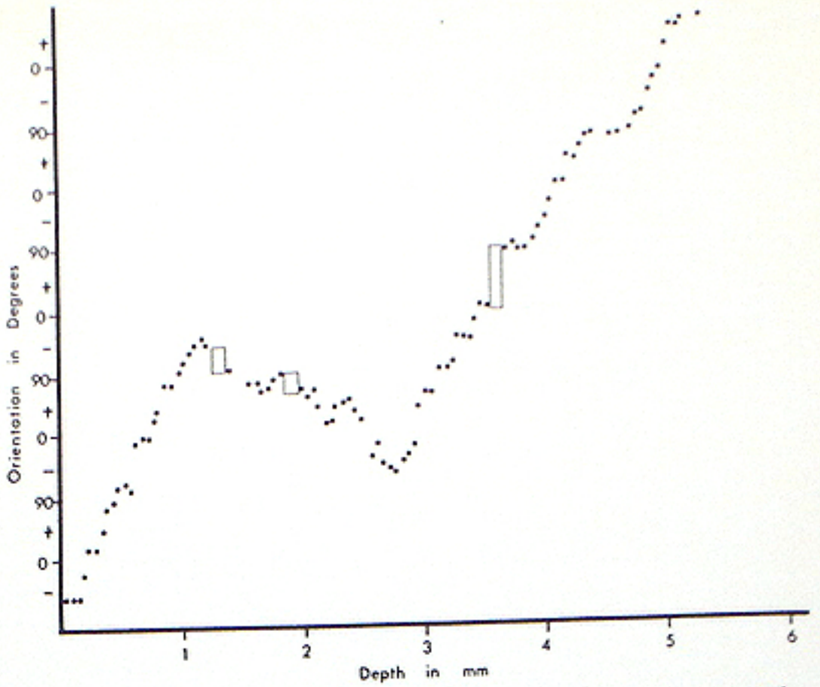

Figure 5. Orientation preferences of units in a single 5-mm-long penetration in layers 2 and 3 of macaque parafoveal striate cortex. The orientation preference changes in a remarkably regular way, with only two reversals in the entire 5 mm. The *rectangles* indicate blobs, where there is no orientation preference, and the sequence continues linearly as if the blob were not there.

from Livingstone and Hubel (1984)

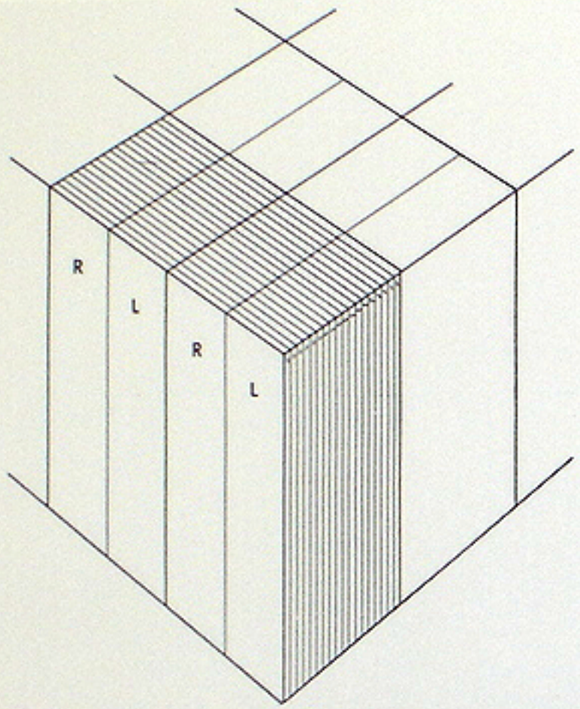

FIGURE 27. Model of the striate cortex, to show roughly the dimensions of the ocular dominance slabs (L, R) in relation to the orientation slabs and the cortical thickness. Thinner lines separate individual columns; thicker lines demarcate hypercolumns, two pairs of ocular dominance columns and two sets of orientation columns. The placing of these hypercolumn boundaries is of course arbitrary; one could as well begin at horizontal or any of the obliques. The decision to show the two sets of columns as intersecting at right angles is also arbitrary, since there is at present no evidence as to the relationship between the two sets. Finally, for convenience the slabs are shown as plane surfaces, but whereas the dominance columns are indeed more or less flat, the orientation columns are not known to be so, and may when viewed from above have the form of swirls.

from Hubel and Wiesel (1977)

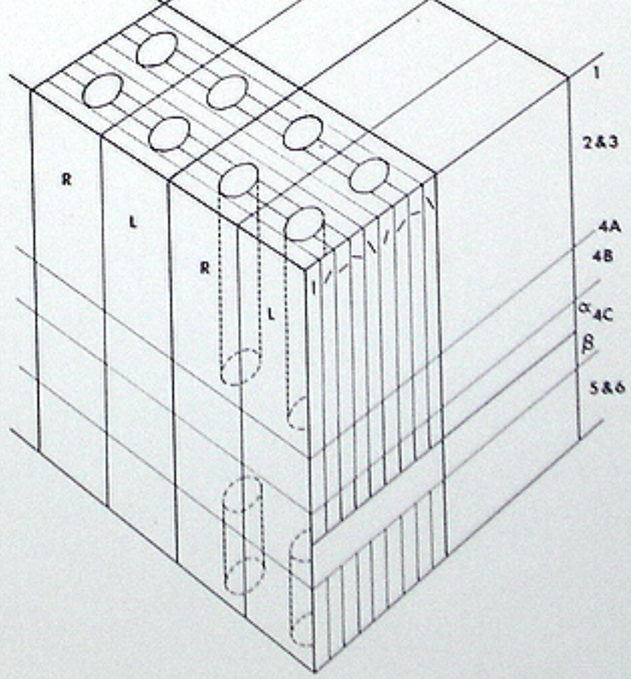

Figure 34. Our current model of the modular organization of macaque striate cortex (modified from Hubel and Wiesel, 1977).

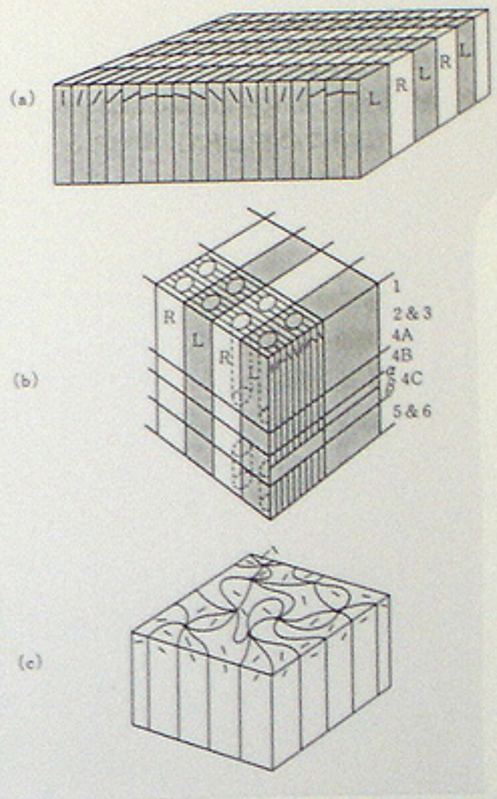

図2-4　V1野の機能構築に関する仮説．Hubel と Wiesel の仮説(a)では，方位選択性と眼優位性は直交するようにV1野の中で表示されている．R：右眼優位のコラム，L：左眼優位のコラム．その後，存在の明らかになったCOブロップを上のモデルに組み込んだのが(b)である．ブロップは4層以外の皮質を貫く円柱状の構造をしており，1つのハイパーコラムあたり4つが埋め込まれている．多数の神経細胞の活動を同時記録できる光学的測定を用いた最近の研究では，方位選択性コラムはその好む傾きに従って，(a)や(b)のモデルのように一直線上に並んでいるのではなく，放射状に並んでいることが明らかになっている(c)．ただし，この構造と眼優位性コラムやCOブロップとの相互関係は明らかでなく，(c)の図にどのように眼優位性コラムやブロップを組み込むかは今後の課題である．

from 藤田 (1994)

受容野の大きさ・拡大因子・ポイントイメージ
(receptive field size, magnification factor, and point image)

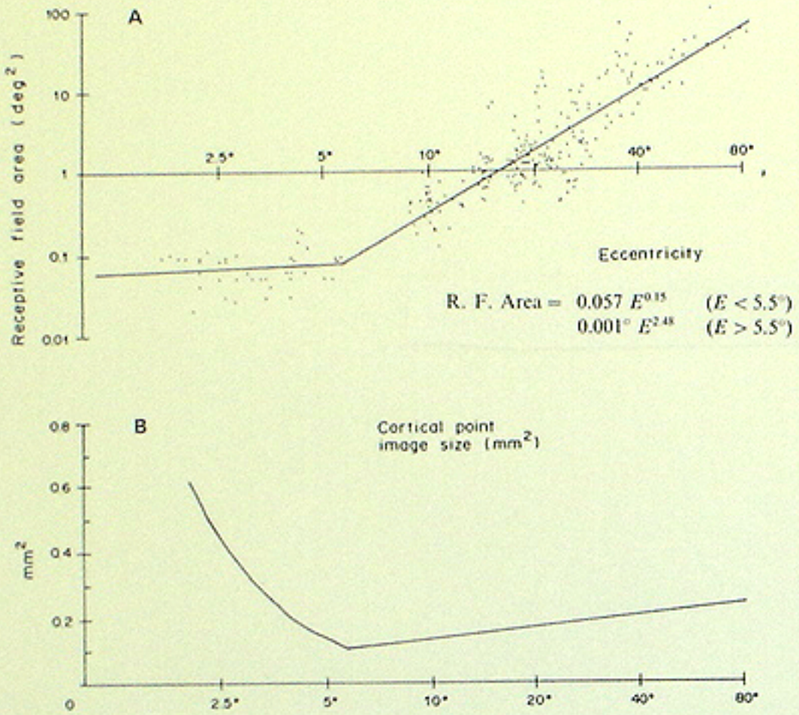

Fig. 7. (A) Receptive field area vs magnification. For binocularly driven responses, separate values are plotted for the left and right eyes. Separate regression lines were calculated for the data above and below 5.5° eccentricity. (B) Cortical point image size (mm^2/deg^2) as a function of eccentricity. The plotted curve equals the product of areal magnification [equation (4)] and multi-unit receptive field area [equation (5)].

from Van Essen et al. (1984)

Mean receptive field sizes of V1 neurons as a function of eccentricity

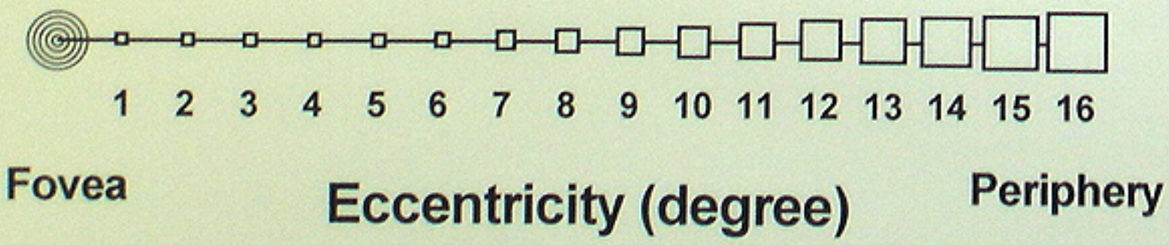

From Van Essen et al. (1984)

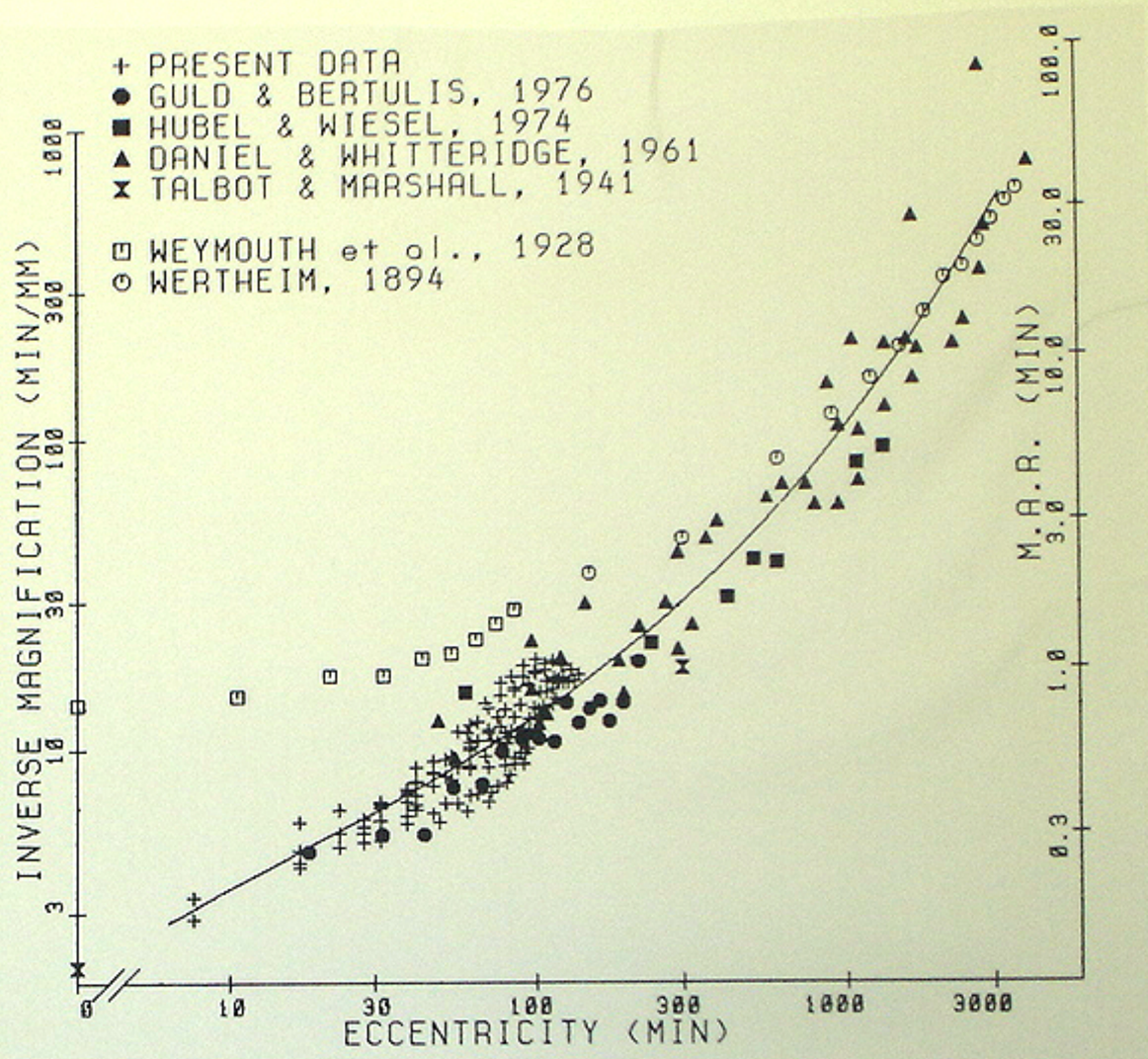

Fig. 6. Inverse magnification in monkey striate cortex as a function of retinal eccentricity from 0° to 50°. Also shown here are minimal angle of resolution data for man (open symbols) plotted on the same coordinate system. The regression line giving log inverse magnification in terms of log eccentricity was obtained by a least squares procedure weighing our points and the previously reported points in ratio 1:3. The result is

$\log_{10} M^{-1} = 0.8124 + 0.5324x + 0.0648x^2 + 0.0788x^3$

where $x = \log_{10} E - 1.5$, and E is expressed in minutes

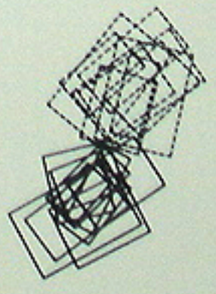

Fig. 4. Overlap of striate receptive fields recorded in pairs of vertical penetrations displaced 2 mm from one another on the cortical surface. For each pair, dashed lines represent receptive fields from one penetration, solid lines represent receptive fields from the other penetration. One pair of penetrations was made in central foveal representation (15' eccentricity), the other in peripheral foveal representation (110' eccentricity)

from Dow et al. (1981)

大細胞系と小細胞系
(magno/parvo system)

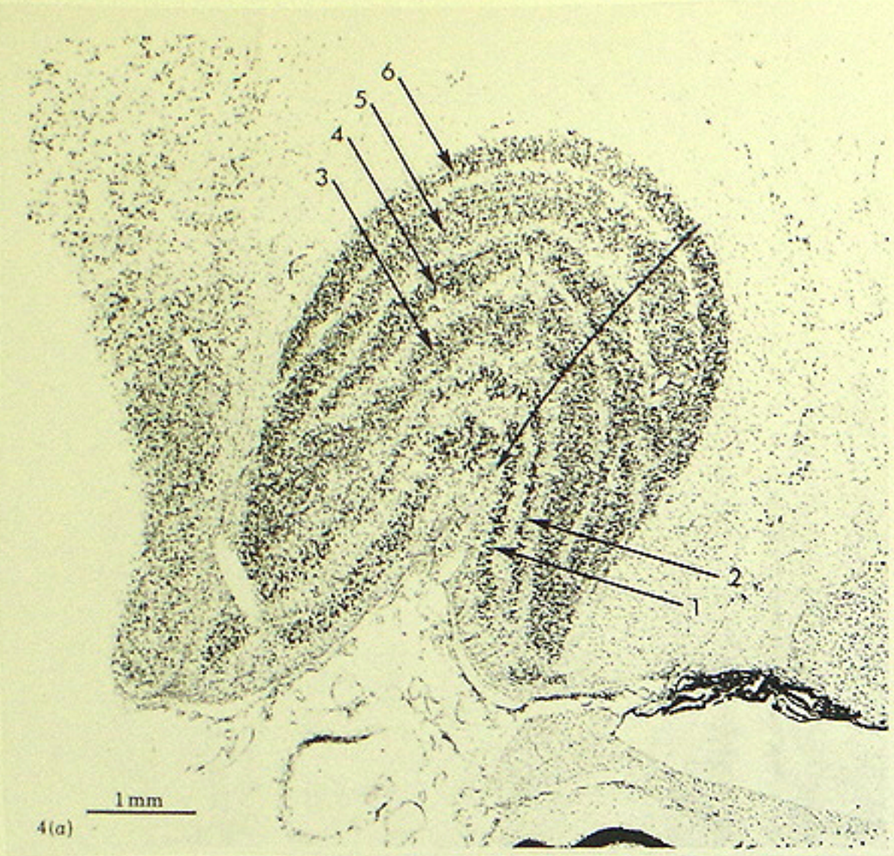

└ from Hubel and Wiesel (1977)

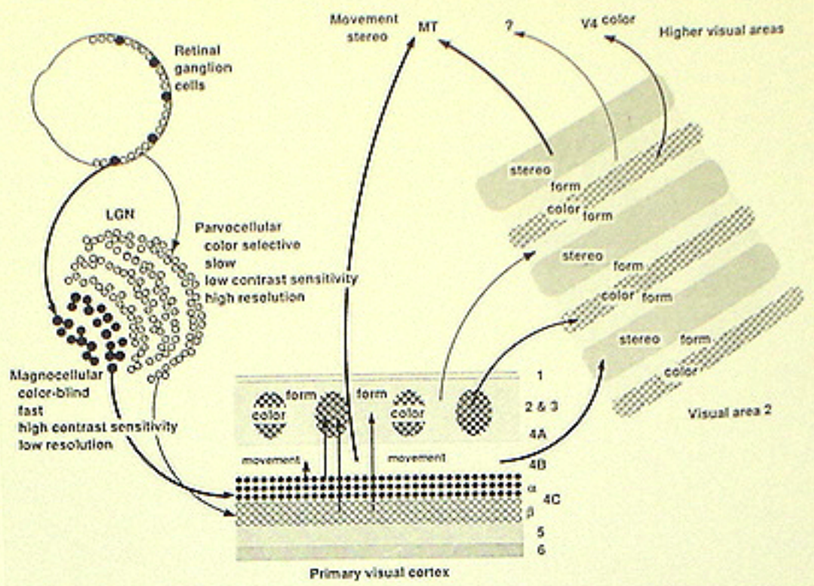

Fig. 4. Diagram of the functional segregation of the primate visual system. MT, middle temporal lobe; V4, visual area 4; LGN, lateral geniculate body.

└ from Livingstone and Hubel (1987)

Table 2. Summary of the major subdivisions and connections of the primate geniculocortical visual system

retina	B-ganglion cells		A-ganglion cells
LGN	parvocellular	interlaminar	magnocellular
Area 17	4C β	?	? 4C α
	interblobs	blobs	4B
Area 18	pale stripes	thin stripes	thick stripes
Higher visual areas	?V3,?V4	V4	MT
Property			
Color	Yes/no[a]	Yes	No
Contrast sensitivity	Low	High[b]	High
Spatial resolution	High	Low	Low
Orientation selectivity	Yes	No	Yes
Movement sensitivity	Yes	No	Yes
Directionality	No[b]	No	Yes[e]
Stereopsis	No[c]	No	Yes

[a] Cells beyond 4Cβ do respond to color-contrast borders but are not overtly color-coded.
[b] At least it is not prominent.
[c] In anesthetized animals, we have seen only a few stereotuned cells in upper-layer area 17 (Livingstone and Hubel, 1984b; see also Hubel and Wiesel, 1970). In attentive animals, cells coded for stereoscopic depth have been reported both above and below layer 4C of area 17, but are especially concentrated in layer 4B (Poggio and Fischer, 1977; Poggio et al., 1985; G. F. Poggio, personal communication). We do not understand these differences in results, but one possibility is that the stereo mechanisms are built up in 18, and the stereotuning in 17 is the result of a back projection that is suppressed by anesthesia.
[d] By deoxyglucose (Tootell et al., 1985).
[e] Rare in thick stripes in area 18 but very common in layer 4B of area 17 and in MT.

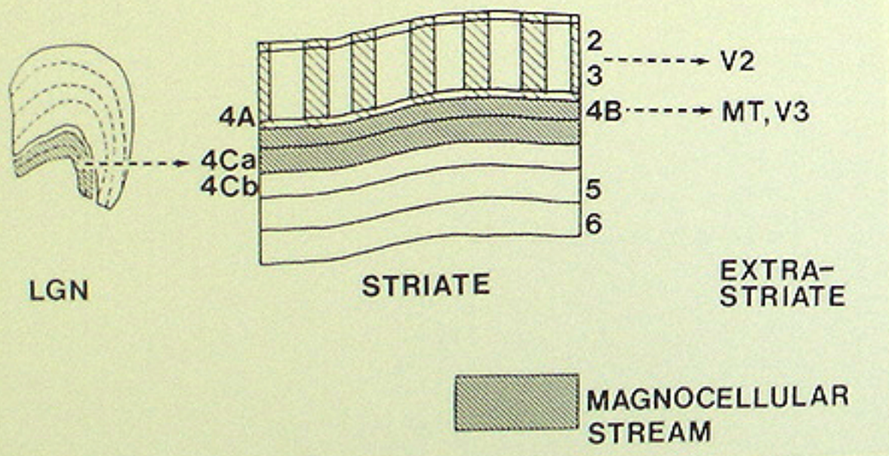

Figure 9. Summary diagram of DG evidence on the flow of magnocellular information through striate cortex. Information from the magnocellular LGN layers projects into 4Ca, and from there it projects into all portions of 4B and weakly into the blobs of layers 2 and 3, and into blob-aligned portions of 4A. Though not shown, magnocellular information also projects strongly into layer 6.

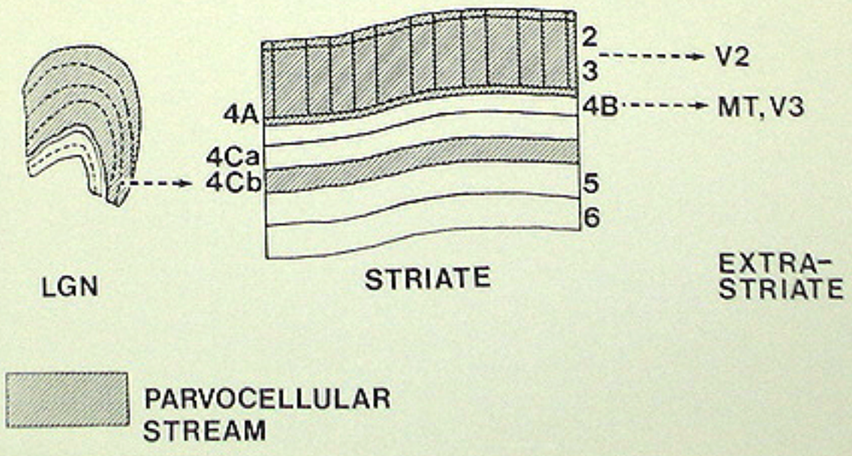

Figure 10. Summary diagram of DG evidence on the flow of parvocellular information through striate cortex. Information from the parvocellular LGN layers projects into striate layers 4Cb and 4A, largely or entirely bypassing layer 4B, projecting richly into all portions of layers 2 and 3. Though not shown, parvocellular information also projects strongly into layers 5 and 6.

from Tootell et al. (1988)

空間周波数コラム
(spatial frequency column)

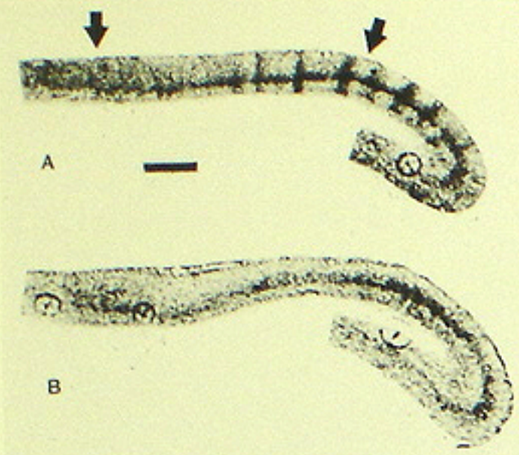

Fig. 1. Comparison of autoradiographs from the striate cortex of two cats. One cat (A) viewed a pattern containing a single spatial frequency (2.0 cycle/deg), and the other (B) a pattern containing multiple spatial frequencies. Both patterns were presented binocularly and at all orientations. Discrete dark columns are seen in the single spatial frequency case (A) but not in the multiple frequency animal (B). In animals that viewed a high-frequency pattern, the columns are restricted to the center of the striate cortex (arrow on right), even though the visual pattern extended in visual space as far as is indicated by the arrow on the left. The autoradiographs are taken from horizontal sections cut at the same depth. Bar is 2 mm.

from Tootell et al. (1982)

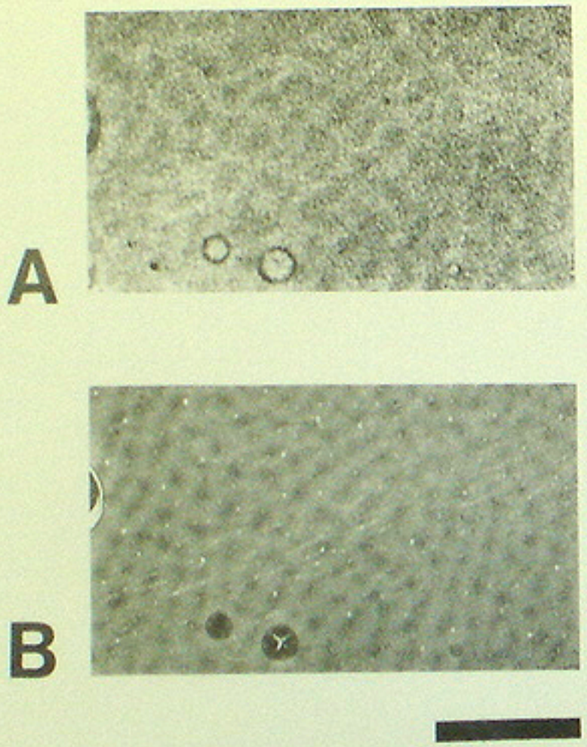

from Tootell et al. (1988)

Figure 3. *A*, Autoradiograph from a monkey presented with a low- (1.5 cycle/deg) spatial-frequency grating at varied orientations, viewed binocularly. Except for the spatial frequency, the stimulus was identical to that used to produce Figure 1*A*. As in Figure 1, the section used to produce Figure 3*A* was taken from striate layer 3, from the representation of eccentricities near 4°–5°. The pattern of cytochrome oxidase staining in the section producing 2A is shown in 2B. Although the contrast of the DG patterns in this case is fairly light, the areas of highest uptake are in general coextensive with regions of high cytochrome oxidase activity. This is more obvious when both images are color-coded and superimposed (see Fig. 2*C*). Calibration bar, 2.5 mm.

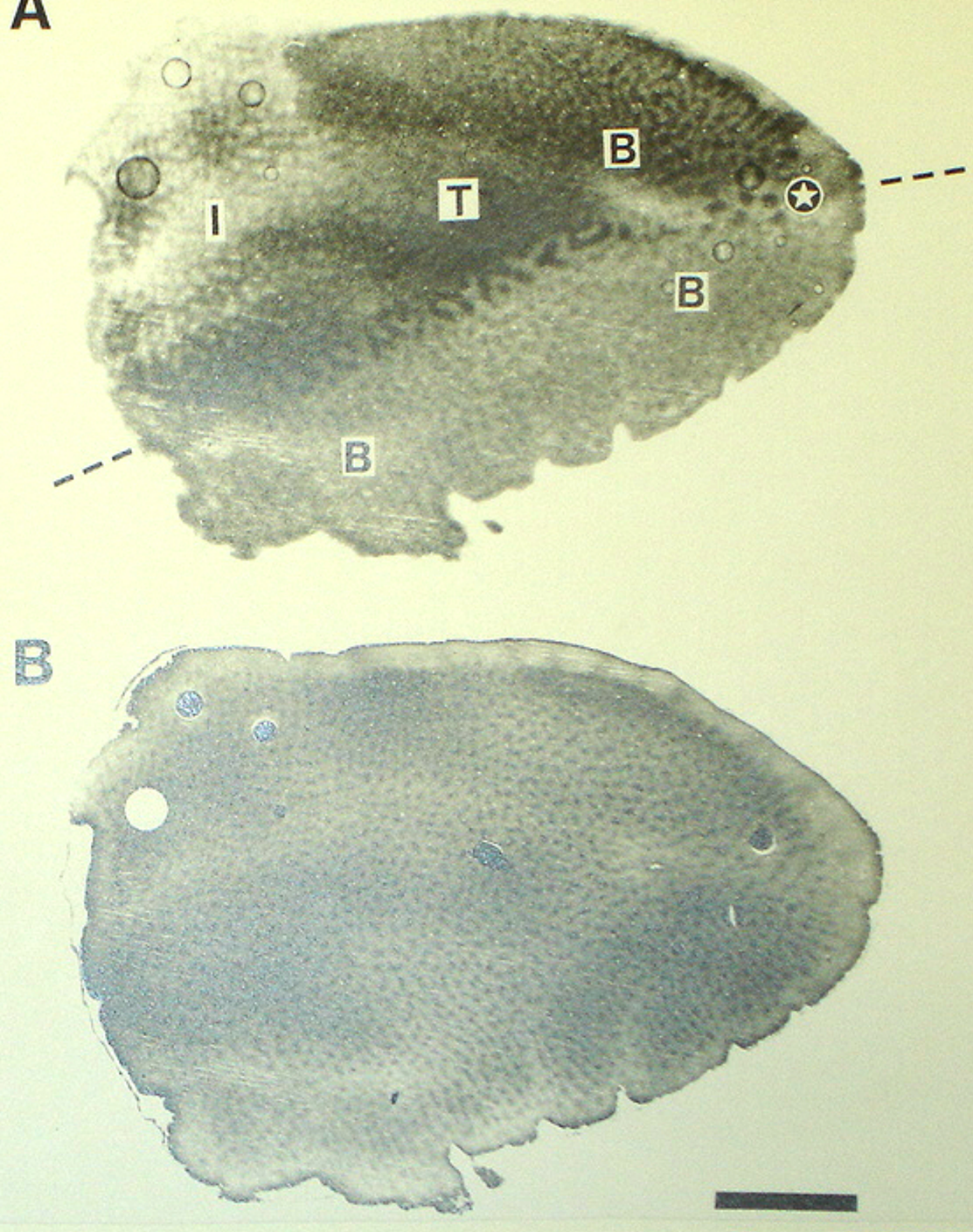

Figure 4. Within-animal comparison of the DG effects of a low- versus a medium–high-spatial-frequency grating. Deoxyglucose autoradiograph (*A*) and the corresponding section stained for cytochrome oxidase (*B*) from a monkey shown gratings of 2 different spatial frequencies in different halves of the visual field. The stimulus consisted of a sinusoidal grating of either 0.9 cycles/deg (above the horizontal meridian) or 4.4 cycles/deg (below the horizontal meridian). Both gratings were presented at a variety of drift rates in both directions, at systematically varied orientations. The eyes were converged as well as possible and the stimulus was shown binocularly. The section used to produce *A* was cut tangential to the flattened cortical surface across the whole lateral operculum. The fovea is represented at the right-most tip of the section (*star*), and more peripheral regions are represented to the *left*. The representation of the horizontal meridian (corresponding to the border between the 2 stimulus halves) can be seen running from the lower left to the upper right through the middle of the section, between the *dashed lines* added outside the section. The visual field is represented in an inverted fashion on striate cortex. The pattern of uptake in the upper half of the section was produced by the 4.4 cycles/deg grating, and the lighter, more *dotted* pattern of uptake in the lower half of the section was produced by the 0.9 cycle/deg grating. The pattern of uptake produced by the 4.4 cycle/deg grating shifts with eccentricity. At the foveal representation (right-most corner), the regions of high uptake overlay the blobs (see Fig. 2*D*), and near 4°–6° eccentricity (*top left*), the regions of high uptake overlay the interblobs (Fig. 2*E*). Between these 2 extremes is a transition region where stimulus-driven DG uptake is high but relatively balanced in blob versus interblob regions (*top, center*). Where DG periodicities overlay the blobs, this is indicated with a *B* in *A*. Where the DG overlays the interblobs, this is indicated with *I*. The transition zone is labelled *T*. Calibration bar, 5 mm.